PCCP

Accepted Manuscript

ROYAL SOCIETY OF CHEMISTRY

www.rsc.org/pccp

Guanine Tetrads: An IRMPD Spectroscopy, Energy Resolved SORI-CID, and Computational Study of M(9-ethylguanine)$_4^+$ (M=Li, Na, K, Rb, Cs) in the Gas Phase

Mohammad Azargun and Travis D. Fridgen*

Department of Chemistry, Memorial University, St. John's, NL, Canada, A1B 3X7

*author to whom all correspondence should be addressed at tfridgen@mun.ca

Abstract

The intrinsic properties of the alkali metal cationized G-tetrads, $M(9eG)_4^+$ (M=Li, Na, K, Rb, Cs) composed of 9-ethylguanine (9eG), were studied by a combination of mass spectrometric techniques. The gas phase structures were probed by infrared multiple photon dissociation (IRMPD) spectroscopy in both the fingerprint region (900 – 1850 cm^{-1}) and the N-H/C-H stretching region (2700 – 3800 cm^{-1}). The gas phase structures were found to be similar for all five complexes and most consistent with the metal-centred G-tetrad structure. Energy-resolved CID was also used to compare the gas phase stabilities of the G-tetrads and showed that $Na(9eG)_4^+$ was more stable than $Li(9eG)_4^+$ followed by the K^+, Rb^+, and Cs^+ G-tetrads in order. The experimental energy ordering was reproduced by electronic structure calculations of the energies. Furthermore, the computations also showed that the lower stability to loss of 9-ethylguanine for the Li^+ complex could be due to a strong destabilization of the neutral G-tetrad due to the persistence toward maximizing the ion-dipole interactions while also maintaining hydrogen bonding interactions.

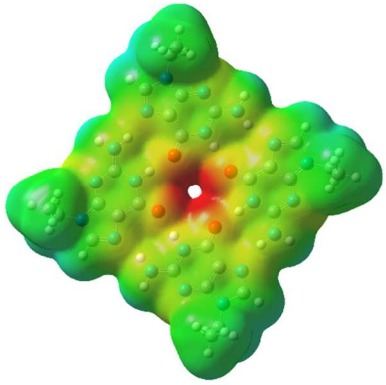

1. Introduction

The guanine nucleobase (Scheme 1A) can form hydrogen-bonded self-assemblies[1,2,3,4] (Scheme 1B) due to its unique arrangement of both a pair of hydrogen donating (N1, NH_2) and accepting (N7, O6) groups. Stable tetrameric clusters, called G-tetrads (or G-quartets), are known to be formed in guanine rich parts of nucleic acids such as DNA.[3] Metal cations are known to facilitate G-tetrad formation.[6] Monovalent metallic cations can be accommodated in the cavity at the centre of the tetrad and bound by the carbonyl oxygen atoms of all four guanines. These metal cations neutralize and stabilize the negative electrostatic potential produced by four oxygen atoms in close proximity.[2,7] The carbohydrate and phosphate backbone make G-tetrad complexes more stackable forming G-quadruplexes.[8,9]

G-tetrad and G-quadruplex clusters have received much attention as they contribute to important biological process.[10,11] At one time, G-quadruplex clusters were believed to be exclusively formed in human telomeric DNA[12,13,14,15] protecting the chromatid from fusing with neighbouring peers and preventing loss of genetic information during replication. Recently, however, research has shown, that G-quadruplexes exist in various locations of human DNA performing numerous functions.[16,17,18,19,20] For instance, Beaudoin and coworkers[20] have studied human mRNA and clearly showed that G-quadruplex can also act as translational suppressor, stopping RNA transcription. In fact, very recently guanine-rich tracks within DNA have been linked to amyotrophic lateral sclerosis (ALS) and frontotemporal dementia (FTD).[21, 22, 23]

Not only do metallic monovalent cations like Li^+, Na^+, and K^+ lower the negative charge density created by the oxygen atoms, but they also can induce formation of these clusters.[4] Further, although it has been commonly accepted that G-tetrads are templated by cations, work

done, in the solution phase using an (N,N-dimethylaniline)guanosine derivative, indicates that clusters can also form in the absence of metal cations.[24] The alkali metal ion affinity of guanine and other nucleobases has been examined in the gas phase by Cerda and coworkers[25] using the kinetic method in which a metallated heterodimer, [nucleobase + B]M^+ where B is a reference base with known cation affinity, is dissociated at different internal energies. The dissociation rates of the hetrodimers into both metalated monomers are compared to obtain the difference in metal cation affinities of monomers. Results show that Li^+ is the most strongly bound alkali metal to guanine, followed by Na^+ and K^+ which shows that these complexes are ion-dipole complexes where the smaller ion has a strong electrostatic interaction. These kinetic method values agree closely with those determined by the threshold collision-induced dissociation (TCID) technique conducted by Rodgers and Armentrout.[26]

Experimental studies in the gas phase along with computational techniques show that the stability of the complexes, G-tetrads and G-quadruplexes, and also their structures correlate with the size of metal cations. The nucleobases in a tetrad rearrange from the planar geometry when a metal cation is present, presumably to maximize ion-dipole interactions while maintaining the strong hydrogen bonding network.[7] Fukushima and Iwahashi[2] concluded that Na^+ is more strongly bound to 9-ethylguanine tetrads than Li^+ and K^+ in the solution phase by comparing peak intensities of the corresponding metal-bound tetrads when a mixture of alkali metal cations and 9-ethylguanine solution was electrosprayed into a mass spectrometer.

Divalent and trivalent cations behave similarly to monovalent cations, forming huge multi-quartet clusters or quadruplexes when exposed to guanine and its derivatives. Cd^{2+}-bound guanosine tetrads were observed following electrospray of a solution of Cd^{2+} and guanosine.[27] In

addition, an electrospray mass spectrometry study performed by Kwan *et al.*[28] reveals that trivalent lanthanide cations like Tb^{3+} can form G-tetrad adducts as well as octameric complexes.

Ion mobility work[29] demonstrated the potency of the ammonium cation to initiate the formation of self-assembled clusters. Sandwich-shaped clusters were observed and their cross-sections were measured and compared to those determined by theoretical methods. Results verify the formation of quadruplexes and G-tetrads in presence of non-metallic cations and more importantly these complexes are stable in solution and keep their structures.

Since the advent of ESI[30], mass spectrometry techniques have become widely used to study non-volatile biological molecules such as nucleobases and their clusters. ESI-MS coupled to a plethora of activation techniques[31,32,33,34,35] have become very useful for studying the intrinsic physical properties of gaseous biological ions. Collisional activation is one of the most common activation techniques.[36,37] Sustained off-resonance irradiation collision-induced dissociation (SORI-CID) is the Fourier transform ion cyclotron resonance mass spectrometry (FT-ICR) version of the CID experiment. It has unique advantages including providing more control on the kinetic energy of parent ions and the ability to increase the activation time resulting in more collisions.[37]

To our knowledge, the intrinsic physical chemistries of alkali metal cation-bound G-tetrad clusters have not been examined or compared experimentally in terms of structures and stability. In this work, we have used the energy-resolved SORI-CID activation technique along with computational chemistry to gain more insight into effect of different alkali metal cations on the structure and energetics of the G-tetrad. The IRMPD spectrum of $Na(Gua)_4^+$ has been recently published, and is consistent with a planar structure in which Na^+ is at the centre of the G-tetrad.[38]

Here, we also present and compare IRMPD spectra in both the fingerprint and N-H/C-H stretching region of G-tetrad complexes with all the alkali metals.

2. Methods

2.1. Experimental. A Bruker ApexQe 7.0 hybrid Fourier transform ion cyclotron resonance (FTICR) mass spectrometer was used to carry out all experiments. 9-ethylguanine was purchased from Sigma-Aldrich and used without further purification like all other chemicals. To prepare solutions, a few drops of 1 mM salt solution (LiCl, NaCl, KCl, RbCl, and CsCl) were added to 10 ml of 0.1 mM 9-ethylguanine solution in 18 MΩ water. The final solution was electrosprayed by an Apollo II ion source coupled to FTICR mass spectrometer at 70-150 μL h^{-1}. SORI-CID experiments were done by isolating the tetramers under study inside the ICR cell (P = 10^{-10} mbar) and exposing them to Ar inside the ICR cell at higher pressures (P ≈ 10^{-5} - 10^{-6} mbar). At these pressures, in the 250 ms excitation time, there are on the order of 10's to 100's of collisions. Since the activation is done by SORI, the kinetic energies vary over the period of excitation and we quote the maximum centre of mass kinetic energies. The average kinetic energies are expected to be 2/3 the maximum kinetic energies. The maximum lab frame kinetic energies are computed using the following equation:[39]

$$E_{\text{lab}}^{\max} = \frac{\beta^2 q^2 V_{p-p}}{32\pi^2 m d^2 \Delta v^2}$$

where B is a geometrical factor of the ICR cell (0.9 in the present case), q is the charge on the ion, $V_{p\text{-}p}$ is the peak to peak excitation voltage, m is the mass of the ion, d is the diameter of the ICR cell (6 cm) and Δν is the frequency offset (500 Hz). The lab frame energies were multiplied

by $m_{\mathrm{Ar}} \Big/ \left(m_{\mathrm{Ar}} + m_{\mathrm{M(9eG)_4^+}} \right)$ to obtain the centre of mass kinetic energies whose maxima ranged from 0.1 to 2.3 eV.

IRMPD experiments were performed by using two setups. IRMPD spectra in the 2700 – 4000 cm^{-1} region were obtained in the Laboratory for the Study of the Energetics, Structures, and Reactions of Gaseous Ions at Memorial University using an IR OPO, manufactured by LaserSpec, tuneable from 1.4 to 4.5 μm, with a bandwidth of 2 cm^{-1}. The OPO is built around a periodically poled lithium niobate crystal which is pumped by a diode pumped solid state Nd:YAG laser. The OPO operates at 20 kHz, with pulse duration of few nanoseconds and generates output power near 3 W at 3 μm. The power was limited to 1 Watt in the present experiments. In the fingerprint region, all experiments were performed using a Fourier-transform ion cyclotron resonance mass spectrometer (FT-ICR-MS) coupled to a mid-infrared free electron laser (FEL) (5 cm^{-1} bandwidth) at the Centre Laser Infrarouge d'Orsay (CLIO).

Unitless IRMPD efficiencies are computed as the negative of the logarithm of the product ion intensities divided by the sum of the total (product + precursor) ion intensities.

2.2. Computational. In this research, the Gaussian 09[40] software package was used to perform all calculations. Hybrid density functional (DFT) techniques have shown their potential and reliability to structurally optimize and also determine the lowest energy structures of nucleobase clusters. B3LYP density functional theory with the 6-31+G(d,p) basis set on C, H, N, and O and the Def2SVPD basis set and ECP's were used on all metals were used for optimizations and calculation of the infrared spectra. Electronic energies were refined using the 6-311+G(3df,3pd) basis on C,H, N, and O and the def2TZVPP basis and ECP on all metals. 298 K relative thermochemistries (enthalpies and Gibbs energies) were calculated from B3LYP/6-

311++G(3df,3pd) electron energies and thermal corrections from the B3LYP/6-31+G(d,p) (note the different basis for all metals as specified above). These thermochemical values are denoted as B3LYP/6-311++G(3df,3pd)//B3LYP 6-31+G(d,p). All dissociation energies were corrected for basis set superposition error using the counterpoise correction method as implemented in G09. All calculations were corrected for dispersion using GD3 empirical corrections.[41]

3. Results and discussion

In this research, 9-ethylguanine was chosen since it is significantly more soluble compared to guanine resulting in mass spectra with improved intensities. Moreover, N9 is blocked by an ethyl group eliminating the possibility for interaction of N9 with the metal cation, blocking it from hydrogen bonding, and prevents it from participating in tautomerization. It is also a better model for biological systems as N9 is the site of glycosylation in nucleic acids.

An electrospray mass spectrum of an aqueous solution prepared by adding only 9-ethylguanine and KCl is shown in Figure 1. The mass spectrum reveals the desired potassiated tetrad, $K(9eG)_4^+$, at m/z 755.3 as well as a potassiated octamer, $K(9eG)_8^+$, at m/z 1471 and the doubly charged ion $K_2(9eG)_{12}^{2+}$ at m/z 1113. Clearly, complexes composed of multiples of four 9-ethylguanines are magic number complexes, with other complexes (i.e. dimeric or trimeric) observed only in minute quantities. To our knowledge, the $K(9\text{-}eG)_8^+$, and $K_2(9\text{-}eG)_{12}^+$, are the largest guanine quadruplexes observed in the gas phase. However, he most abundant ion observed is the sodiated tetrad, $Na(9\text{-}eG)_4^+$, at m/z 739. The observation of $Na(9\text{-}eG)_4^+$ when Na^+ is only present as an impurity is consistent with previous work concluding the exceptional solution phase stability of the $Na(9\text{-}eG)_4^+$ over tetrads associated with other metal cations.[2] It

should also be noted that despite the large intensity of $Na(9\text{-}eG)_4^+$, no larger clusters are observed. This is the topic of a future manuscript on guanine quadruplexes.

3.1 Computed Structures of Metalated G-Tetrads, $M(9eG)_4^+$.

The computed structures of the G-tetrads are summarized in Figure 2 with structural parameters provided in Table 1. Individual snapshots of each $M(9eG)_4^+$ structure are given in Figure S1. In all cases the O—O distances are significantly shorter compared to the neutral G-tetrad. The addition of Li^+ to the neutral G-tetrad shrinks the O—O distance by almost 1 Δ due to strong ion-dipole interactions. In $Na(9eG)_4^+$ the O—O distance is shortened by about 0.5 Δ and for the largest ion, Cs^+, the distance is only shorter by a few hundredths of an angstrom compared to the neutral tetramer. The greater contraction of the tetrad with the smaller sized alkali metal cation is consistent with ion-dipole interactions occurring between the metal cation and the 9-ethylguanines. The NH—N hydrogen bond is also shorter for all the metal cation/G-tetrad complexes due to the increasing ionic nature of the hydrogen bond by addition of the charged metal. Interestingly, the NH—N hydrogen bond is the shortest in $Na(9eG)_4^+$, of all the complexes. The NH—O hydrogen bond increases slightly upon the addition of a metal cation which is expected since the metal cation is also bound to the oxygen atom in each of the 9-ethylguanines. $Na(9eG)_4^+$ is the only planar G-tetrad other than the neutral complex. $Li(9eG)_4^+$ is very different from the other structures as the Li^+ sits inside a rather twisted G-tetrad in order to maximize the ion-dipole interactions but also to relieve any repulsion that would be present by not allowing the hydrogen bonds to get too short, yet maintaining the strong hydrogen bonds. For K^+, Rb^+, and Cs^+, the metal cation sits on top of a non-planar, slightly distorted G-tetrad. The larger the metal cation, the higher above the tetrad the metal cation sits as indicated by the πOOM angle. There are also two values for each of the structural parameters listed for the K^+,

Rb^+, and Cs^+ complexes. That is due to the complexes resembling, somewhat, two 9eG dimers in those tetraplexes.

3.2 IRMPD Spectroscopy $M(9eG)_4^+$.

The IRMPD spectra for the $M(9eG)_4^+$ tetrads are compared to each other and to the computed spectra for the lowest-energy structures in both the 2700 – 3800 cm^{-1} and the 900 – 1850 cm^{-1} regions in Figure 3. The experimental spectra for all of the $M(9eG)_4^+$ are quite similar to one another in both regions, indicating similarities in their structures. In fact, there really is no way to distinguish between the complexes composed of a different alkali metal cations based on the IRMPD spectra. More importantly, the IRMPD spectra and the computed IR spectra for the lowest energy structures are in very good agreement although there is one observed band in the high energy region that is not accounted for by the computed IR spectra and will be discussed below. We also note that the present experimental spectrum of $Na(9eG)_4^+$ is in good agreement with the those of $Na(guanine)_4^+$ which was concluded to belong to a planar complex similar to the lowest energy complex shown in Fig. 2 for $Na(9eG)_4^+$.[38]

In the lower energy region, the most prominent band is at 1680 cm^{-1} due to C=O stretching and C-N-H bending and a resolved shoulder at about 1615 cm^{-1} due to C-N-H bending. There is also a band at 1375 cm^{-1} due to C-NH_2 stretching and CH_2 wagging. Between these main absorptions are three weak features (at ~1480, 1535, and 1575 cm^{-1}) due mainly to C-C and C-N stretching. Another weak band is observed at 1190 cm^{-1} due to deformation and C-N stretching. In the higher energy region, the main absorption occurs at about 3180 cm^{-1} and is due to the hydrogen bonded N-H stretching vibrations. The highest energy band occurs at 3515 cm^{-1}

is due to the free N-H stretch (or antisymmetric stretch of the NH_2 group). These calculations predict this band to be at a slightly higher wavenumber position, about 3570 cm^{-1}. Harmonic calculations have been shown to overestimate the wavenumber position of the antisymmetric NH_2 stretch of adenine, a similar purine base,[42,43,44] as well as cytosine.[45] Anharmonic calculations were shown to correctly reproduce the position of the NH_2 antisymmetric stretch and our own anharmonic frequency calculations on $Na(9eG)_4^+$ predict the NH_2 stretch to occur at 3502 cm^{-1}, in better agreement with the experimentally observed band. There is a strong band observed at 3330 cm^{-1} as well as a shoulder to the 3180 cm^{-1} band, at 3240 cm^{-1} that are resolved for the Na^+, K^+, Rb^+ and Cs^+ clusters and have no fundamental band predicted in these regions. An obvious possibility for these bands are overtones of the very strong C=O stretching absorption observed at 1680 cm^{-1}. Fraschetti *et al.* used *ab initio* molecular dynamics simulations[38] to show that these two absorptions could also belong to the hydrogen bonded N-H stretches of a rapidly fluctuating structure due to a very flat potential energy surface for distortion in and out of planarity of this non-covalently bonded complex.

In Figure S2 the experimental spectra for $Na(9eG)_4^+$, $Li(9eG)_4^+$, and $K(9eG)_4^+$ are compared to computed spectra for the lowest energy isomer and two higher energy isomers that we were able to find and optimize. One of the isomers has Hoogsteen-type pairing, but with only three 9-ethylguanines, the fourth is bound to the metal through O6 and N7. These isomers are 56, 85, and 61 kJ mol^{-1} higher in Gibbs energy than the lowest energy isomer for the Li^+, Na^+, and K^+ tetrads. An even higher energy isomer has the metal cation bound to all four 9-ethylguanines through N7 and interactions between O6 and H8, and is more than 140 kJ mol^{-1} higher in Gibbs energy relative to the lowest energy structure. The best matches to the experimental spectra are the lowest energy G-tetrad structures. We conclude therefore, that the

IRMPD spectra point to very similar G-tetrad-like structures with Hoogsteen base pairing in the gas phase for all five $M(9eG)_4^+$ complexes, those shown in Fig. 2/S1.

3.3 Relative Gas-Phase Stabilities of the $M(9eG)_4^+$ Tetrads by Energy-Resolved SORI-CID.

Energy-resolved SORI-CID activation was used to determine the relative stabilities of the alkali metal cationized G-tetrads. After isolation, the G-tetrads were excited to collision energies of between 0 and 0.7 eV and exposed to Ar gas with a reservoir pressure of argon of 10 mbar. In Figure S3 are the breakdown diagrams for all five complexes. This figure shows that in all cases, the complexes dissociate losing sequential 9-ethyl guanine molecules as the trimer intensity occurs at lower energy than the dimer intensity followed by a rise in the monomer intensity. Only in the case of the Cs^+ cluster is the bare ion observed and only at the highest collision energies. It would not be possible to observe signal for the bare metal cations of Li^+ or Na^+ due to the low mass cut-off of the ICR due to the frequency generator. However, we note that in the K^+ or Rb^+ experiments over the energy range studied, no bare metal cations were observed. We cannot completely rule out the direct loss of a neutral dimer from the $M(9eG)_4^+$ complexes. For example, for $Na(9eG)_4^+$ there is only a small accumulation of $Na(9eG)_3^+$ and the most abundant product is $Na(9eG)_2^+$. This means that on a relative basis, it may be more energetically feasible to lose a neutral dimer than a neutral monomer.

In Figure 4 the $M(9eG)_4^+$ intensities, for all five G-tetrads, are plotted against the collision energy. A line is drawn parallel to the energy axis at 50% dissociation of the G-tetrads. It is apparent that $Na(9eG)_4^+$ requires the greatest energy to affect 50% dissociation, followed by $Li(9eG)_4^+$ and then the K^+, Rb^+ and Cs^+ G-tetrads. On the basis of ion dipole interactions

between the metal cations and guanine, the gas-phase stabilities of the tetrads would be expected to follow the order $Li^+ > Na^+ > K^+ > Rb^+ > Cs^+$ due to the decreasing charge density of the metal cation.[25,26]

The experiments were repeated with an Ar reservoir pressure of 5 and 15 mbar (Figure S4), effectively decreasing and increasing the pressure inside the ICR cell. The energies required to affect dissociation were observed to increase at the lower pressure and decrease at the higher pressure due to a decreased and increased, respectively, collision frequency as expected. The ordering of the energy required to dissociate $M(9eG)_4^+$ was the same at all three energies, $Na^+ > Li^+ > K^+ > Rb^+ > Cs^+$. In Figure 5, the relative centre of mass energies to affect 50% dissociation are plotted along with the computed dissociation enthalpies for the following reaction:

$$M(9eG)_4^+ \rightarrow M(9eG)_3^+ + 9eG$$

It is clear from Figure 5 that the energy resolved SORI-CID experiments and theory agree that the Na^+ tetrad is the most stable to dissociation. This agrees with conclusions from solution phase studies by simply electrospraying solutions containing 9-ethylguanine and all the metal cations at the same concentration.[2]

The computed 298 K dissociation enthalpies for both levels of theory are summarized in Table 2. As well, single-point calculations were done on the complexes, but after removing the metal cation. These energies (all computed with the larger basis) were compared to the energies of the neutral complex and were found to be 63.3, 30.9, 23.9, 21.9, and 20.2 kJ mol^{-1} for the Li^+, Na^+, K^+, Rb^+, and Cs^+ complexes, respectively. These energies are destabilization energies, the effect of the metal cation on the energy of the neutral G-tetrad by distorting it from its normal geometry. Clearly, the twisted and compact structure of $Li(9eG)_4^+$ has the largest effect,

distorting the tetrad, and raising its energy, by the greatest amount. Na^+ distorts the tetrad by the next greatest amount followed by K^+, Rb^+, and Cs^+. If these energies are added to the dissociation energies of the $M(9eG)_4^+$ complexes and the dissociation energy of the neutral tetrad itself (37.1 kJ mol^{-1}) is removed, the resulting value (the last column of Table 2) represents the amount (at least relatively) by which the metal cation stabilizes the G-tetrad to loss of a neutral 9-eG. The trend for these values is a monotonic decrease as the size of the metal cation increases or the charge density decreases as would be expected for a purely ion-dipole complex. These calculations show that the secondary effect of the metal cation, distorting the G-tetrad to maximize ion-dipole interactions while maintaining hydrogen bonding interactions, seems to be the reason for $Li(9eG)_4^+$ being less stable than $Na(9eG)_4^+$ in the gas phase.

4. Conclusions.

We have investigated gas phase structures and relative stabilities of the alkali metal cationized G-tetrads, $M(9eG)_4^+$ (M=Li, Na, K, Rb, Cs). These intrinsic properties were studied by a combination of mass spectrometric techniques. IRMPD spectroscopy in both the fingerprint region (900 – 1850 cm^{-1}) and the N-H/C-H stretching region (2700 – 3800 cm^{-1}) showed that the gas phase structures for all five complexes are most consistent with the metal-centred G-tetrad structure and that they are all give very similar IRMPD spectra. Calculations also predict very similar IR spectra in both regions studied. Energy-resolved SORI-CID was used to compare the gas phase stabilities of the G-tetrads and showed that $Na(9eG)_4^+$ is the most stable in agreement with solution phase studies. The stability of the other four complexes were found to decrease in the order $Li(9eG)_4^+ > K(9eG)_4^+ > Rb(9eG)_4^+ > Cs(9eG)_4^+$. This experimental energy ordering

was reproduced by electronic structure calculations of the energies. Based upon the charge density of the ions it was expected that the Li^+ G-tetrad might be more stable than the Na^+ G-tetrad. Calculations were used to show that the lower stability to loss of 9-ethylguanine for the Li^+ complex could be due to a strong distortion and therefore destabilization of the neutral G-tetrad due to maximizing ion-dipole interactions while also maintaining hydrogen bonding interactions.

The present study does not explain why it is the potassium ion that is most commonly associated with G-quadruplexes in DNA, but we hope to answer that question in a forthcoming article.

5. Acknowledgements.

The authors wish to express their gratitude for ongoing funding from the Natural Sciences and Engineering Research Council of Canada. Infrastructure funding from the Canadian Foundation for Innovation, the Industrial Research and Innovation Fund, and Bruker are gratefully acknowledged for funds to build the Laboratory for the Study of the Energetics, Structures, and Reactions of Gaseous Ions at Memorial University. The authors wish to thank the CLIO team (J.M. Ortega, C. Six, G. Perilhous, J. P. Berthet) as well as P. Maître and V. Steinmetz for their support during the experiments. We also thank Dr. Andre Peremans (LaserSpec) for his expertise and ongoing support with the OPO laser. Finally, the authors also acknowledge the computational resources provided by ACE-Net and Westgrid.

Figure Captions

Figure 1. Electrospray mass spectrum of 10 mL of 0.1 mM solution of 9-ethylguanine to which two drops of 0.1 mM KCl was added.

Figure 2. Computed structures of the metal cationized G-tetrads indicating the structural parameters listed in Table 1.

Figure 3. IRMPD spectra of the M(9eG)4+ G-tetrads in the 900 – 1850 cm^{-1} and the 2700 – 3800 cm^{-1} regions (black traces). The underlying grey traces are the computed spectra (B3LYP/6-31+G(d,p), Def2SVPD on metals) for the lowest energy G-tetrad structures scaled by 0.97 in both regions. The insets for the fingerprint regions of the Na^+ and K^+ tetramers are without an attenuating element, roughly 10x the laser intensity.

Figure 4. Tetramer intensity vs the centre of mass energy decay curve for the $M(9eG)_4^+$ G-tetrads from the energy-resolved SORI-CID spectra experiments. Reservoir pressure was 10 mbar with Ar. The higher energy required to dissociate $Na(9eG)_4^+$ indicates a structure more stable to loss of 9-ethylguanine.

Figure 5. The relative centre of mass collision energies to affect 50 % dissociation for the five alkali metal cationized G-tetrads. The experimental values were done at three different reservoir

pressures as indicated in the legend. The white bars show the computed binding energies for loss of a 9-ethylganine from $M(9eG)_4^+$. The computed values are from the B3LYP/6-311+G(3df,3pd) calculations listed in Table 2.

Table 1. B3LYP/6-31+G(d,p) structural parameters for the $M(9eG)_4^+$ guanine tetrads, M=Li, Na, K, Rb, and Cs, and $(9eG)_4$.

Species	O-O	NH—N	NH—O	M-O	πOOM
$(9eG)_4$	4.991	1.970	1.755		
$Li(9eG)_4^+$	3.947	1.895	1.776	2.031	13.9
$Na(9eG)_4^+$	4.582	1.866	1.839	2.291	0.0
$K(9eG)_4^+$	4.781/4.847	1.888/1.897	1.855/1.864	2.655/2.660	24.1/26.0
$Rb(9eG)_4^+$	4.797/4.898	1.886/1.901	1.844/1.856	2.838/2.846	30.4/32.6
$Cs(9eG)_4^+$	4.841/4.946	1.889/1.911	1.829/1.844	3.028/3.046	35.2/38.5

Table 2. 298 K Dissociation enthalpies of neutral and alkali metal cationized G-tetrads, $(9eG)_4$ and $M(9eG)_4^+$.

Species	B3LYP/ 6-31+G(d,p)[a]	B3LYP/ 6-311+G(3df,3pd)[b]	Remove G-tetrad distortion energy[c]
$(9eG)_4$	37.5	37.1	
$Li(9eG)_4^+$	106.8	133.8	160.0
$Na(9eG)_4^+$	136.3	163.4	157.2
$K(9eG)_4^+$	104.2	131.4	118.2
$Rb(9eG)_4^+$	98.6	127.8	112.6
$Cs(9eG)_4^+$	88.1	118.8	101.9

a: Def2SVPD on metal cations and empirical dispersion

b: Def2TZVPP on metal cations and empirical dispersion

c: calculated using B3LYP/6-311(3df,3pd) and the calculations in column 3.

References

1. T. J. Pinnavaia, H. T. Miles and E. D. Becker, *J. Am. Chem. Soc.*, 1975, **97**, 7198-7200.
2. K. Fukushima and H. Iwahashi, *Chem. Commun.*, 2000, 895-896.
3. J. T. Davis and G. P. Spada, *Chem. Soc. Rev.*, 2007, **36**, 296-313.
4. K. J. Koch, T. Aggerholm, S. C. Nanita and R. Graham Cooks, *J. Mass Spectrom*, 2002, **37**, 676-686.
5. M. Meyer, M. Brandl and J. Sühnel, *J. Phys. Chem. A*, 2001, **105**, 8223-8225.
6. N. Campbell and S. Neidle, in *Interplay between Metal Ions and Nucleic Acids*, eds. A. Sigel, H. Sigel and R. K. O. Sigel, Springer Netherlands, 2012, vol. 10, pp. 119-134.
7. S. Mezzache, S. Alves, J.-P. Paumard, C. Pepe and J.-C. Tabet, *Rapid Commun. Mass Spectrom.* , 2007, **21**, 1075-1082.
8. J. T. Davis, *Angew. Chem. Int. Ed.*, 2004, **43**, 668-698.
9. S. Burge, G. N. Parkinson, P. Hazel, A. K. Todd and S. Neidle, *Nucleic Acids Res.*, 2006, **34**, 5402-5415.
10. M. Métifiot, S. Amrane, S. Litvak and M.-L. Andreola, *Nucleic Acids Res.* , 2014.
11. Y. Wu and R. M. Brosh, *FEBS J.*, 2010, **277**, 3470-3488.
12. S. Neidle and G. N. Parkinson, *Curr. Opin. Struct. Biol.*, 2003, **13**, 275-283.
13. T. K. Pandita, in *Encyclopedia of Cancer (Second Edition)*, ed. R. B. Editor-in-Chief: Joseph, Academic Press, New York, 2002, pp. 353-361.
14. F. W. Smith and J. Feigon, *Nature*, 1992, **356**, 164-168.
15. P. Balagurumoorthy and S. K. Brahmachari, *J. Biol. Chem.*, 1994, **269**, 21858-21869.
16. A. Siddiqui-Jain, C. L. Grand, D. J. Bearss and L. H. Hurley, *Proc. Natl. Acad. Sci. U.S.A.*, 2002, **99**, 11593-11598.
17. R. De Armond, S. Wood, D. Sun, L. H. Hurley and S. W. Ebbinghaus, *Biochemistry*, 2005, **44**, 16341-16350.
18. T. Simonsson, M. Kubista and P. Pecinka, *Nucleic Acids Res.*, 1998, **26**, 1167-1172.
19. J. L. Huppert, A. Bugaut, S. Kumari and S. Balasubramanian, *Nucleic Acids Res.*, 2008, **36**, 6260-6268.
20. J.-D. Beaudoin and J.-P. Perreault, *Nucleic Acids Res.*, 2010, **38**, 7022-7036.

21. A. R. Haeusler, C. J. Donnelly, G. Periz, E. A. J. Simko, P. G. Shaw, M.-S. Kim, N. J. Maragakis, J. C. Troncoso, A. Pandey, R. Sattler, J. D. Rothstein and J. Wang, *Nature*, 2014, **507**, 195-200.
22. A. E. Renton, E. Majounie, A. Waite, J. Simón-Sánchez, S. Rollinson, J. R. Gibbs, J. C. Schymick, H. Laaksovirta, J. C. van Swieten, L. Myllykangas, H. Kalimo, A. Paetau, Y. Abramzon, A. M. Remes, A. Kaganovich, S. W. Scholz, J. Duckworth, J. Ding, D. W. Harmer, D. G. Hernandez, J. O. Johnson, K. Mok, M. Ryten, D. Trabzuni, R. J. Guerreiro, R. W. Orrell, J. Neal, A. Murray, J. Pearson, I. E. Jansen, D. Sondervan, H. Seelaar, D. Blake, K. Young, N. Halliwell, J. Callister, G. Toulson, A. Richardson, A. Gerhard, J. Snowden, D. Mann, D. Neary, M. A. Nalls, T. Peuralinna, L. Jansson, V.-M. Isoviita, A.-L. Kaivorinne, M. Hölttä-Vuori, E. Ikonen, R. Sulkava, M. Benatar, J. Wuu, A. Chiò, G. Restagno, G. Borghero, M. Sabatelli, I. C. The, D. Heckerman, E. Rogaeva, L. Zinman, J. Rothstein, M. Sendtner, C. Drepper, E. E. Eichler, C. Alkan, Z. Abdullaev, S. D. Pack, A. Dutra, E. Pak, J. Hardy, A. Singleton, N. M. Williams, P. Heutink, S. Pickering-Brown, H. R. Morris, P. J. Tienari and B. J. Traynor, *Neuron*, 2011, **72**, 257-268.
23. M. DeJesus-Hernandez, I. R. Mackenzie, B. F. Boeve, A. L. Boxer, M. Baker, N. J. Rutherford, A. M. Nicholson, N. A. Finch, H. F. Gilmer, J. Adamson, N. Kouri, A. Wojtas, P. Sengdy, G.-Y. R. Hsiung, A. Karydas, W. W. Seeley, K. A. Josephs, G. Coppola, D. H. Geschwind, Z. K. Wszolek, H. Feldman, D. Knopman, R. Petersen, B. L. Miller, D. Dickson, K. Boylan, N. Graff-Radford and R. Rademakers, *Neuron*, 2011, **72**, 245-256.
24. J. L. Sessler, M. Sathiosatham, K. Doerr, V. Lynch and K. A. Abboud, *Angew. Chem. Int. Ed.* , 2000, **39**, 1300-1303.
25. B. A. Cerda and C. Wesdemiotis, *J. Am. Chem. Soc.*, 1996, **118**, 11884-11892.
26. M. T. Rodgers and P. B. Armentrout, *J. Am. Chem. Soc.*, 2000, **122**, 8548-8558.
27. H. Moriwaki, *J. Mass Spectrom.*, 2003, **38**, 321-327.
28. I. C. M. Kwan, Y.-M. She and G. Wu, *Chem. Commun.*, 2007, 4286-4288.
29. E. S. Baker, S. L. Bernstein and M. T. Bowers, *J. Am. Soc. Mass Spectrom.*, 2005, **16**, 989-997.
30. J. Fenn, M. Mann, C. Meng, S. Wong and C. Whitehouse, *Science*, 1989, **246**, 64-71.

31. T. D. Fridgen, *Mass Spectrom. Rev.*, 2009, **28**, 586-607.
32. N. C. Polfer and J. Oomens, *Mass Spectrom. Rev.*, 2009, **28**, 468-494.
33. R. C. Dunbar, *Mass Spectrom. Rev.*, 2004, **23**, 127-158.
34. E. A. L. Gillis, M. Demireva, K. Nanda, G. Beran, E. R. Williams and T. D. Fridgen, *Phys. Chem. Chem. Phys.*, 2012, **14**, 3304-3315.
35. W. D. Price, P. D. Schnier and E. R. Williams, *Anal. Chem.*, 1996, **68**, 859-866.
36. L. Sleno and D. A. Volmer, *J. Mass Spectrom.* , 2004, **39**, 1091-1112.
37. J. Laskin and J. H. Futrell, *Mass Spectrom. Rev.*, 2003, **22**, 158-181.
38. C. Fraschetti, M. Montagna, L. Guarcini, L. Guidoni and A. Filippi, *Chem. Commun.*, 2014, **50**, 14767-14770.
39. C. Peltz, L. Drahos and K. Vékey, *J. Am. Soc. Mass Spectrom.*, 2007, **18**, 2119-2126.
40. M. J. F. e. al, *Gaussian, Inc., Wallingford, CT*, 2009.
41. S. Grimme, S. Ehrlich and L. Goerigk, *J. Comput. Chem.*, 2011, **32**, 1456-1465.
42. C. Mao, T. H. LaBean, J. H. Reif and N. C. Seeman, *Nature*, 2000, **407**, 493-496.
43. K. Rajabi, E. A. L. Gillis and T. D. Fridgen, *J. Phys. Chem. A*, 2010, **114**, 3449-3456.
44. E. A. L. Gillis and T. D. Fridgen, *Int. J. Mass spectrom.*, 2010, **297**, 2-8.
45. F. Wang, M. T. Downton and N. Kidwani, *J. Chem. Theory Comput.*, 2005, **04**, 247-264.

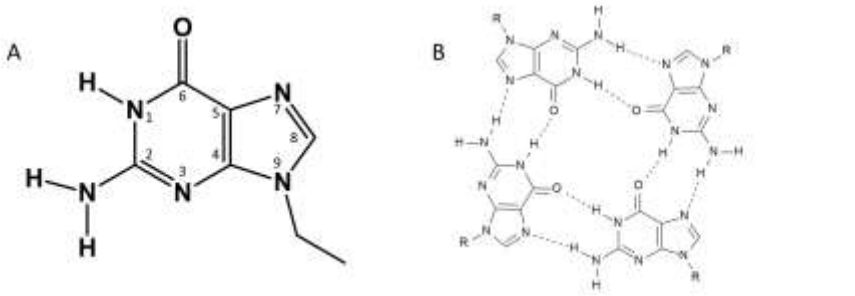

Scheme 1.

254x190mm (300 x 300 DPI)

Figure 1.

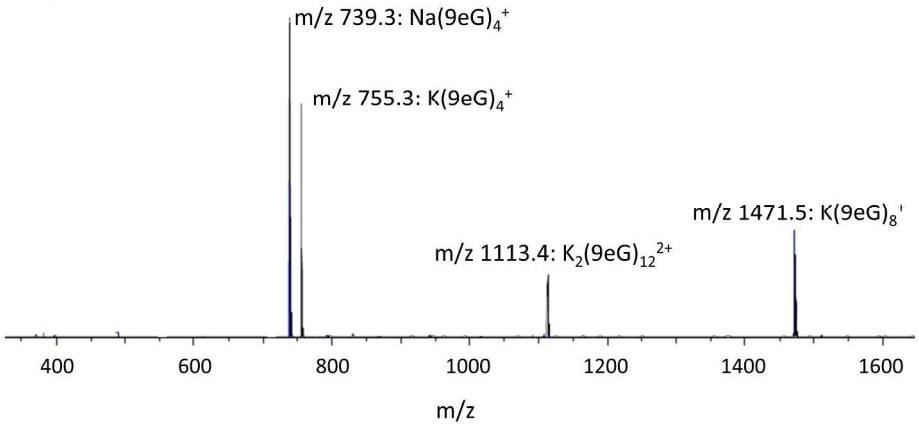

Electrospray mass spectrum of 10 mL of 0.1 mM solution of 9-ethylguanine to which two drops of 0.1 mM KCl was added.
254x190mm (300 x 300 DPI)

Figure 2.

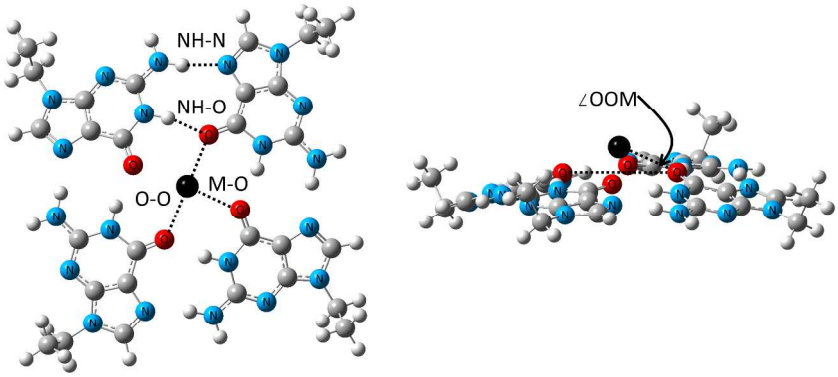

Computed structures of the metal cationized G-tetrads indicating the structural parameters listed in Table 1.
254x190mm (300 x 300 DPI)

Figure 3.

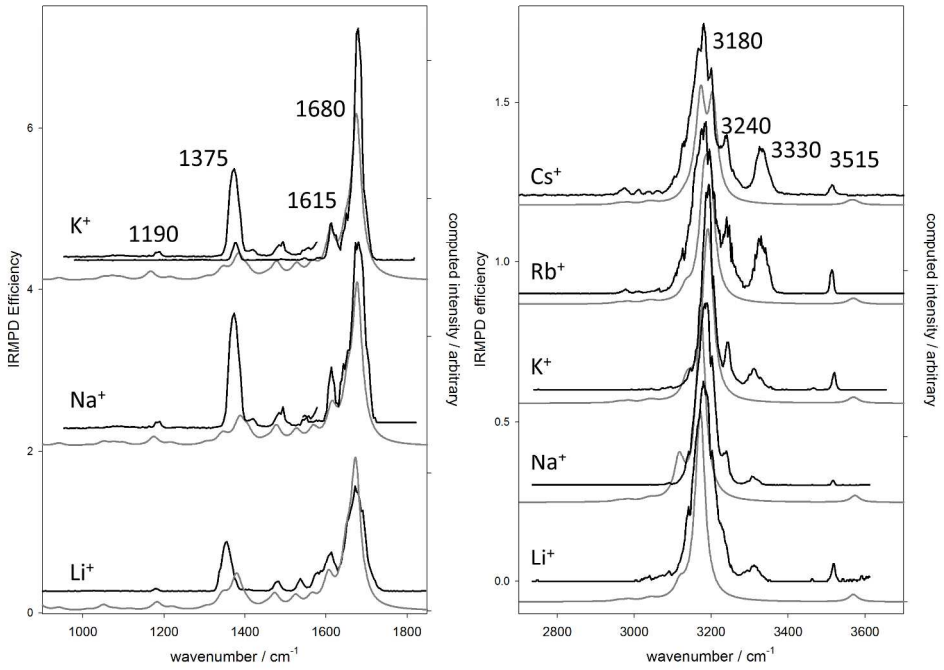

. IRMPD spectra of the M(9eG)4+ G-tetrads in the 900 – 1850 cm-1 and the 2700 – 3800 cm-1 regions (black traces). The underlying grey traces are the computed spectra (B3LYP/6-31+G(d,p), Def2SVPD on metals) for the lowest energy G-tetrad structures scaled by 0.97 in both regions. The insets for the fingerprint regions of the Na+ and K+ tetramers are without an attenuating element, roughly 10x the laser intensity.
254x190mm (300 x 300 DPI)

Figure 4.

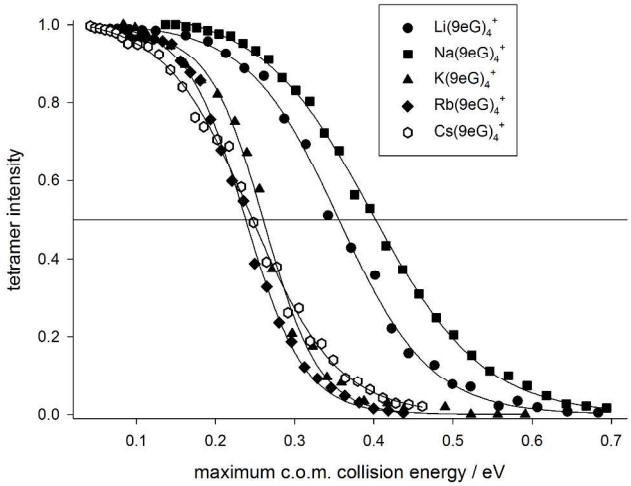

Tetramer intensity vs the centre of mass energy decay curve for the M(9eG)4+ G-tetrads from the energy-resolved SORI-CID spectra experiments. Reservoir pressure was 10 mbar with Ar. The higher energy required to dissociate Na(9eG)4+ indicates a structure more stable to loss of 9-ethylguanine.
254x190mm (300 x 300 DPI)

Figure 5.

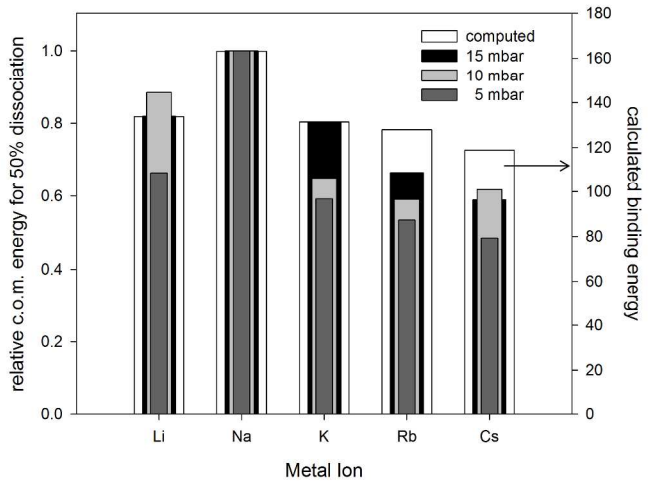

The relative centre of mass collision energies to affect 50 % dissociation for the five alkali metal cationized G-tetrads. The experimental values were done at three different reservoir pressures as indicated in the legend. The white bars show the computed binding energies for loss of a 9-ethylganine from M(9eG)4+.
254x190mm (300 x 300 DPI)